Imaging and Analysis of Individual Cavitation Microbubbles around Dental Ultrasonic

Vyas, Nina; Sammons, Rachel; Walmsley, Anthony; Wang, Qian; Dehghani, Hamid; Leppinen, David

DOI:
10.1016/j.ultras.2017.05.015

Ultrasonics 81 (2017) 66–72

Contents lists available at ScienceDirect

Ultrasonics

journal homepage: www.elsevier.com/locate/ultras

Imaging and analysis of individual cavitation microbubbles around dental ultrasonic scalers

N. Vyas [a,b], H. Dehghani [c], R.L. Sammons [b], Q.X. Wang [d], D.M. Leppinen [d], A.D. Walmsley [b,*]

[a] Physical Sciences of Imaging for Biomedical Sciences (PSIBS) Doctoral Training Centre, College of Engineering & Physical Sciences, University of Birmingham, Birmingham B15 2TT, UK
[b] School of Dentistry, College of Medical and Dental Sciences, University of Birmingham, Mill Pool Way, Birmingham B5 7EG, UK
[c] School of Computer Science, University of Birmingham, Edgbaston, Birmingham B15 2TT, UK
[d] School of Mathematics, University of Birmingham, Edgbaston, Birmingham B15 2TT, UK

ARTICLE INFO

Article history:
Received 11 January 2017
Received in revised form 23 May 2017
Accepted 23 May 2017
Available online 24 May 2017

Keywords:
Cavitation bubbles
Bubble analysis
Piezoelectric devices
Image processing
High speed imaging
Ultrasonic dental scalers

ABSTRACT

Cavitation is a potentially effective and less damaging method of removing biofilm from biomaterial surfaces. The aim of this study is to characterise individual microbubbles around ultrasonic scaler tips using high speed imaging and image processing. This information will provide improved understanding on the disruption of dental biofilm and give insights into how the instruments can be optimised for ultrasonic cleaning. Individual cavitation microbubbles around ultrasonic scalers were analysed using high speed recordings up to a million frames per second with image processing of the bubble movement. The radius and rate of bubble growth together with the collapse was calculated by tracking multiple points on bubbles over time. The tracking method to determine bubble speed demonstrated good inter-rater reliability (intra class correlation coefficient: 0.993) and can therefore be a useful method to apply in future studies. The bubble speed increased over its oscillation cycle and a maximum of 27 ms^{-1} was recorded during the collapse phase. The maximum bubble radii ranged from 40 to 80 μm. Bubble growth was observed when the ultrasonic scaler tip receded from an area and similarly bubble collapse was observed when the tip moved towards an area, corresponding to locations of low pressure around the scaler tip. Previous work shows that this cavitation is involved in biofilm removal. Future experimental work can be based on these findings by using the protocols developed to experimentally analyse cavitation around various clinical instruments and comparing with theoretical calculations. This will help to determine the main cleaning mechanisms of cavitation and how clinical instruments such as ultrasonic scalers can be optimised.

1. Introduction

The dynamics of individual cavitation bubbles are of interest to many scientific disciplines including hydraulics (propellers, turbines and pumps), ultrasound cleaning and biomedical engineering. The aim is to understand the mechanisms underlying the surface cleaning, erosion and sonoporation effects [1]. The characteristics of microbubbles around dental ultrasonic scalers are directly related to cavitation cleaning behaviour but the exact mechanisms are not fully understood [2]. Current methods of dental plaque biofilm removal are predominantly mechanical and are not effective in removing it from irregular surfaces in the mouth. Cavitation occurring around dental ultrasonic scalers may be a more efficient and less damaging technique. Previous work has failed to quantify the cavitation bubble dynamics around ultrasonic scalers and its effects. Understanding the cavitation bubble dynamics could help to provide insights into how the cavitation can clean biofilms. This will enable manufacturers to develop instruments that optimise the cavitation cleaning effects [3].

High speed imaging of bubbles combined with image analysis is a non-intrusive method of experimentally investigating cavitation, and can provide detailed information on bubble structure without interfering with their dynamic activity [4–7]. A considerable amount of literature has been published on the mathematical modelling of individual cavitation bubble behaviour to understand how they clean or erode surfaces [8–16]. Chahine et al. simulated bubbles near different boundaries (rigid, elastic and free surface) to measure the pressure driving the bubble and found that the distance between the bubble and the surface to be cleaned influenced the cleaning [17]. Theoretical calculations have also been combined with experimental validation using high speed imaging [10,18]. These studies have calculated the evolution of the bubble

* Corresponding author at: School of Dentistry, University of Birmingham, Mill Pool Way, Birmingham B5 7EG, UK.
E-mail address: a.d.walmsley@bham.ac.uk (A.D. Walmsley).

http://dx.doi.org/10.1016/j.ultras.2017.05.015
0041-624X/

radius over time and modelled the diffusion inside the liquid for different applications such as drug delivery and erosion. However no such research has been conducted on cavitation bubbles from ultrasonic scalers.

A range of phenomena have been identified which occur during the collapse of cavitation bubbles and may contribute to their cleaning effect. If a cavitation bubble collapses near a boundary, such as a wall or another bubble, it will form a high velocity micro liquid jet which penetrates through the centre of the bubble and impacts the opposite surface with large local stresses [8]. The re-entrant jet penetrates the bubble at a higher velocity than the rest of the collapsing bubble surface, impacting the opposite surface at speeds of over 100 m/s and a pressure of ~400 MPa [19]. It is believed that the jet and resulting shock wave imposes a localised high hydrodynamic load on the solid surface nearby, removing the biofilm off the surface [1]. In terms of damage from erosion, Phillip and Lauterborn identified that the jet only has an effect when the bubble is very near to or touching the surface, and that the main mechanism is the formation of a vortex ring bubble (a torus shaped bubble rotating poloidally) which collapses producing high pressure pulses [10,19]. This may also contribute to ultrasonic cleaning but the exact bubble dynamics which lead to biofilm removal remain to be elucidated [1]. Cavitation bubbles can also lyse cellular membranes and could kill bacterial biofilm as well as disrupting it, but the cellular pathways which occur in bacteria when cavitation is applied have not yet been identified [1,20].

Quantitative research on cavitation around endodontic files has been done using high speed particle imaging velocimetry and computational fluid dynamics to show the fluid flow and acoustic microstreaming occurring around the files [21,22]. In terms of high speed imaging to study cavitation around dental instruments, individual microbubbles have been imaged around endodontic files and lasers [23–26]. Peeters et al. showed how air trapped in a root canal can be released and Matsumoto et al. showed that more cavitation occurred in an enclosed root canal model compared to in free space. Macedo et al. used high speed imaging to demonstrate cavitation occurring at the end of endodontic files, and qualitatively observed how the cavitation cloud changed with different irrigant solutions [27]. However these studies have not performed image analysis of individual cavitation bubbles due to the limited temporal and spatial resolution. In addition, very little is known about the characteristics of individual cavitation bubbles around ultrasonic scalers. Bubble dynamics around ultrasonic scaler tips have not yet been studied using high speed imaging combined with image processing. Observing bubble phenomena will help to determine the timescales of growth and collapse, how this is affected by scaler power settings and where nucleation sites are located. This will contribute to discovering how cavitation microbubbles cause biofilm disruption.

The aim of this study is to characterise individual microbubbles around ultrasonic scaler tips using high speed imaging and image processing. Specifically, we aim to observe cavitation bubble phenomena and calculate bubble speed and radius during the growth and collapse phases.

2. Materials and methods

2.1. High speed imaging

An ultrasonic scaler (P5 Newtron, Satelec, Acteon, France) was imaged with tip 10P at various power settings (Power 5, 7, 10, 15, 20 (maximum)) using high speed cameras. It should be noted that the power control dial of the ultrasonic scaler is not a reproducible measure of power. The power output of the ultrasonic scaler cannot be measured accurately due to the tip shape, however Walmsley et al. have shown that the displacement amplitude of the tip is that main factor which has to be controlled [28,29]. The displacement amplitude of the tip is given in Vyas et al [30].

A Photron SA1.1 high speed camera (Photron, San Diego, CA, USA) was used to image bubbles at 250 k frames per second (fps) or 500 kfps. The camera was attached to a zoom lens (Monozoom 7, Leica Microsystems UK Ltd) to obtain a resolution of 5.6 μm/pixel. The size of each pixel was calculated from measurements of a 2 mm graticule with 10 μm markings. More information about the experimental setup using the Photron camera is given in Vyas et al. [30].

To give more details about the bubble collapse phase, an ultra-fast high speed camera (HPV1, Shimadzu Corporation, Japan) was used to image cavitation microbubbles around tip 10P at 1,000,000 fps. The camera was attached to a zoom lens (Monozoom 7, Leica Microsystems UK Ltd) to obtain a resolution of 6.7 μm/pixel (Fig. 1). The size of each pixel was calculated from measurements of a 2 mm graticule with 10 μm markings. The difference in resolution between the two imaging systems is due to differences in their focal lengths. Illumination was provided by two strobe lights which were synchronised with the camera using a flash light controller, delay generator and trigger switch. The scaler was positioned using a translation stage (PT3, Thorlabs, USA). The scaler tip was imaged in a custom-made glass container with a total volume of 10 ml. The container was made by cutting glass microscope slides to 2.7 × 2.7 mm and attaching 5 squares to each other using glass adhesive (Loctite, USA) to create an open cube. The scaler tip was submerged in the container in 10 ml reverse osmosis water at 20.5 °C.

2.2. Image analysis

All image analysis was done using Fiji (distribution of the ImageJ software, US National Institutes of Health, Bethesda, Maryland, USA) [31]. Data graphing was done using SigmaPlot 12.3 (Systat Software, USA) and statistical analysis was performed using SPSS (IBM, USA). The image analysis steps described below are also summarised in Supplementary Figure S1.

Image sequences where individual bubbles were seen to grow and collapse completely within the imaging field of view were used to extract the outline of the bubbles for further analysis. These images were first cropped and segmented using the Trainable Weka Segmentation Plugin [32]. Some parts of the background were falsely segmented and were eliminated by removing objects smaller than 4 pixels using the Analyse particles plugin. Objects touching the edge of the image were also removed (using the 'exclude on edges' feature in the Analyse particles plugin) to remove other bubbles which were partially in the field of view. The outline of the bubble was then created using the 'outline' function in the Binary menu of Fiji. For the cases where there were multiple individual bubbles in the images, a watershed segmentation was performed to separate bubbles in the image which were touching each other before creating an outline of the binary bubble shapes. These steps were completed for all time points during a bubble's growth and collapse.

The x-y coordinates of the binary outline of two bubbles were saved for an image sequence with an inter-frame time of 2 μs and plotted as a 3D graph to visualise the bubble localisation during the different stages. 3D visualisation (with the 3rd dimension being time) was also done using the 3D viewer in Fiji for multiple individual bubbles observed simultaneously. To aid in visualisation through time, the image sequence was colour coded to show the different bubble behaviour at different time points.

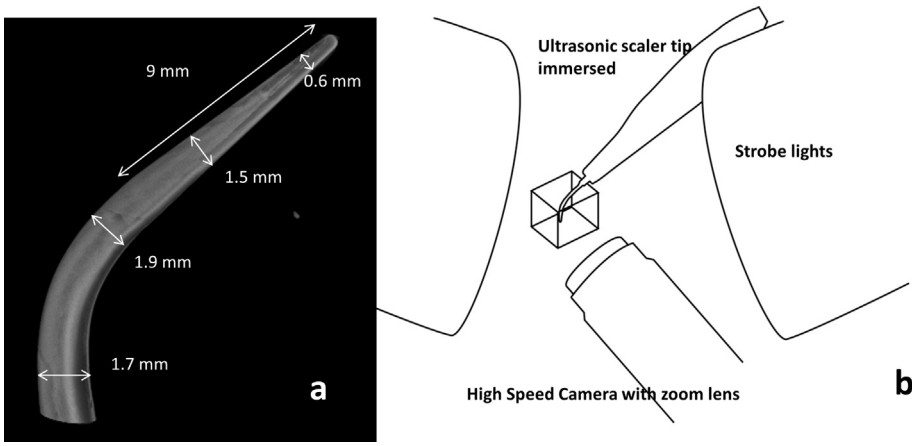

Fig. 1. (a) Micro computed tomography 3D reconstruction of Tip 10P with dimensions, (b) schematic of the experimental setup showing the ultrasonic scaler tip in its imaging container with the zoom lens and strobe lights.

2.2.1. Calculating bubble radius

The equivalent radius of a bubble at each time point was calculated and plotted as a function of time from the binary images of the bubbles. Circularity was assumed to calculate the equivalent radius (r):

$$r = \sqrt{A/\pi}$$

where A is the bubble area. The assumption of spherical bubbles in this study is valid for most of their life cycle except during collapse, which is asymmetrical. It is difficult to accurately perform calculations of an asymmetric bubble because the internal gas dynamics and the fluid mechanics of the liquid need to be taken into account.

2.2.2. Calculating speed of bubble wall

Bubble growth and collapse speed was calculated using the MTrackJ manual tracking plugin in Fiji [33]. Tracking was done at 8 locations on the binary outline of the bubble for each time point and the mean speed was calculated. The locations on the edge of the bubble were chosen to be equispaced approximately every 45°. The inter-rater reliability of the manual tracking was found using the intra class correlation coefficient (ICC). Seven operators performed manual tracking of one bubble as described above to test the reproducibility of the tracking method when performed by different people. The average speed of the bubble at each time point was calculated from the 8 tracks. The different speeds obtained by the different users were compared using the ICC.

3. Results

Transient cavitation was observed in all high speed videos, i.e. microbubbles continuously grew and collapsed. Stable cavitation (where bubbles oscillate over many cycles without collapsing) was not observed. Typical bubble behaviour at the end of tip 10P is shown in Fig. 2. One or two individual bubbles first grew and collapsed. After their collapse, many more bubbles or a bubble cloud emerged at the same location of the previous bubble during the next oscillation cycle of the ultrasonic scaler tip (Fig 2, supplementary video S1). The cavitation then formed into a cluster of bubbles growing and collapsing at the end of the tip. Groups of cavitation microbubbles can be seen around tip 10P at different power settings of the ultrasonic scaler (Fig. 3). At low power (Fig. 3a) cavitation can be seen at one point on the tip. At medium powers (Fig. 3b & c) more cavitation occurs around the whole end of the

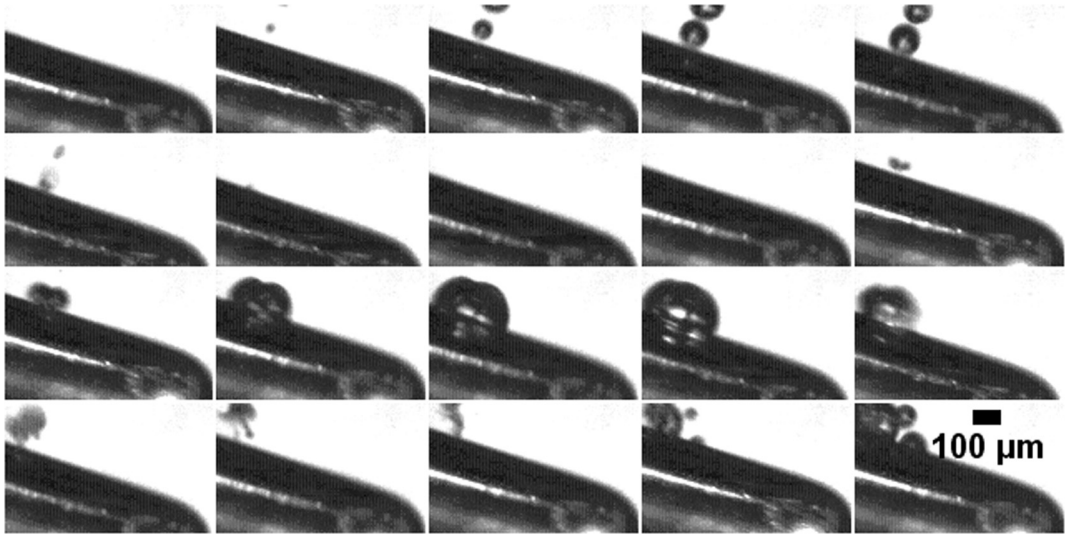

Fig. 2. Image sequences of bubbles growing and collapsing around at the end of tip 10P. Images show an example of multibubble growth, collapse and regrowth. Inter-frame time: 4 μs. Power setting: 10.

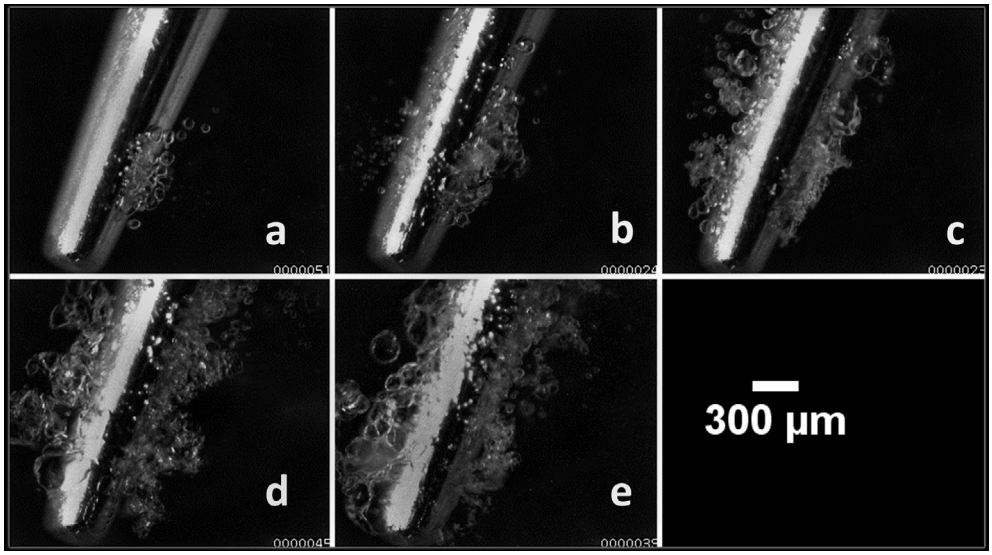

Fig. 3. High speed images of microbubbles around 10P at various power settings (a) power 5, (b) power 7, (c) power 10, (d) power 15, (e) power 20 (maximum power setting).

tip and at the higher powers (Fig. 3d & e) it increases further, with larger microbubbles.

The 3D plot in time of individual microbubble outlines shows the non-linear bubble collapse which starts at one point on the bubble (Fig. 4). In Fig. 4(b) the bubble rebounds for 1 microsecond after the first collapse before disappearing. This is not observed in Fig. 4(a).

There were more cavitation clouds around the tip rather than individual bubbles. A group of individual microbubbles could be seen in one high speed video (Fig. 5, highlighted by the rectangle).

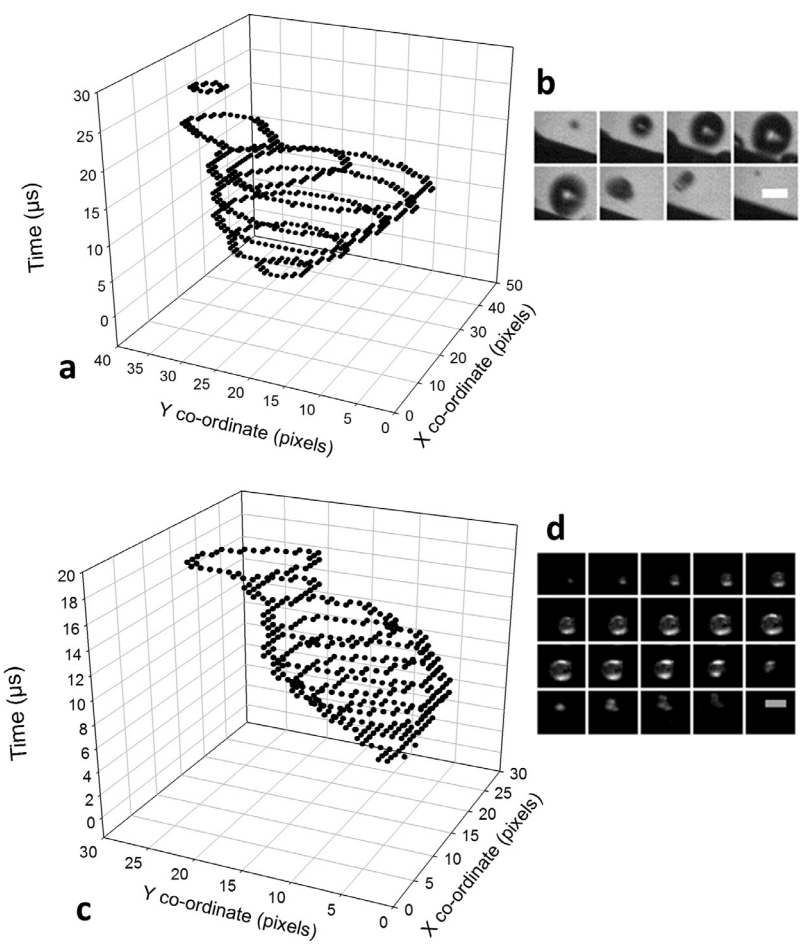

Fig. 4. (a, c) 3D plots in time of the x-y coordinates of bubble outlines as they grow and collapse, showing the position of the bubble at each time point. The origin in the graphs refers to the top left corner of the high speed image. Images from cavitation around tip 10P at power 10. (b, d) Corresponding original cropped images from high speed video. Scale bar represents 100 μm.

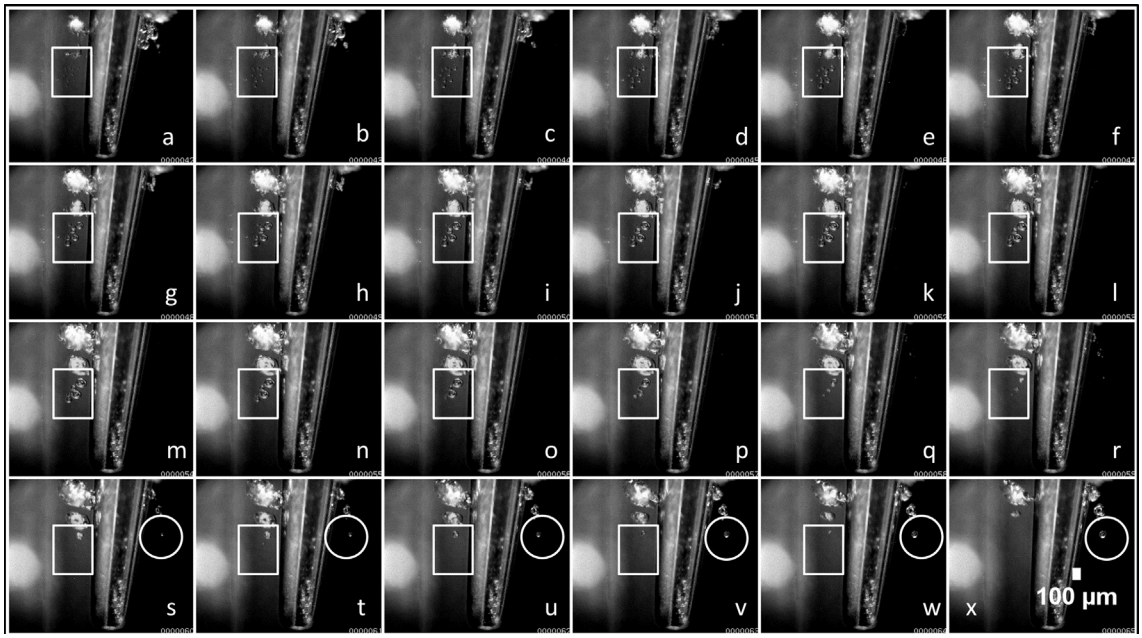

Fig. 5. Image sequence of a group of microbubbles around tip 10P at power 10 (highlighted in rectangle, also see supplementary video S2) and an individual micro bubble (circled). Time difference between frames is 1 µs.

The evolution of these bubbles over time can be visualised more clearly in supplementary video S2. They start as small microbubbles shown in magenta, and then evolve to the larger microbubbles shown in cyan and green. One of these jets upwards (shown in yellow) before collapsing.

Fig. 6(a) shows an example of the manual tracking done with MTrackJ and the tracks drawn by an operator at 8 points on the bubble. The single measures ICC for the manual tracking was 0.993 (Fig. 6b). An example of the bubble outline extracted from the image sequences is shown in Fig. 6(c) in magenta overlaid on

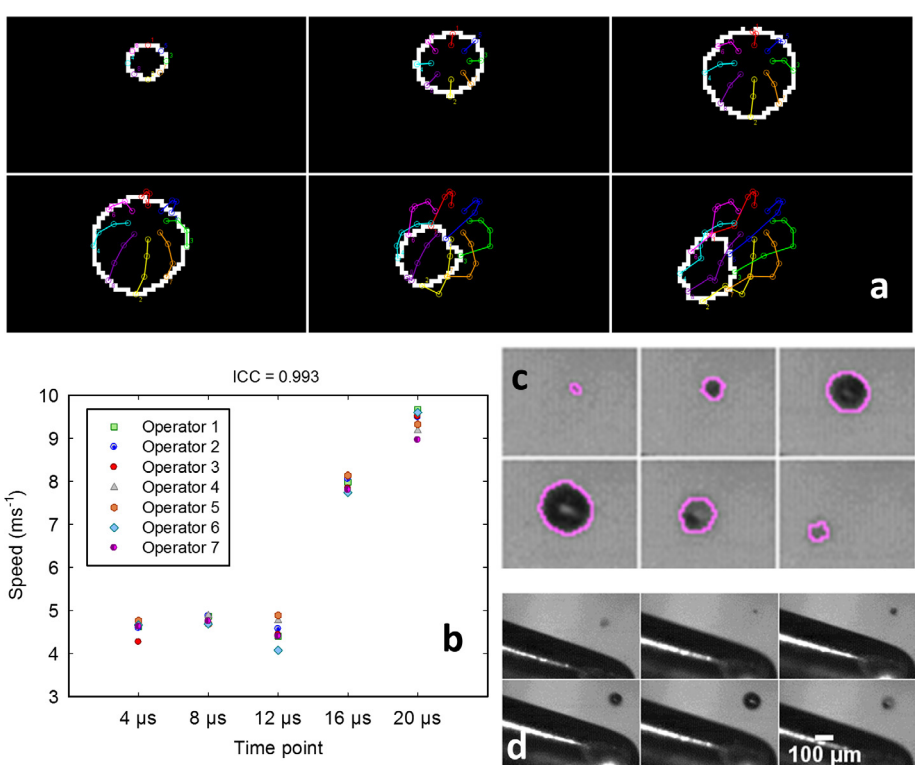

Fig. 6. (a) Example of the MTrackJ plugin showing the tracks at 8 points on a bubble as it grows and collapses, (b) Dot plot showing the mean speed measurements from 7 operators at each time point, (c) Example of an individual bubble used for tracking, with the binary outline overlaid in magenta, (d) Original image sequence of the bubble near the free end of tip 10P. Frame interval is 4 µs.

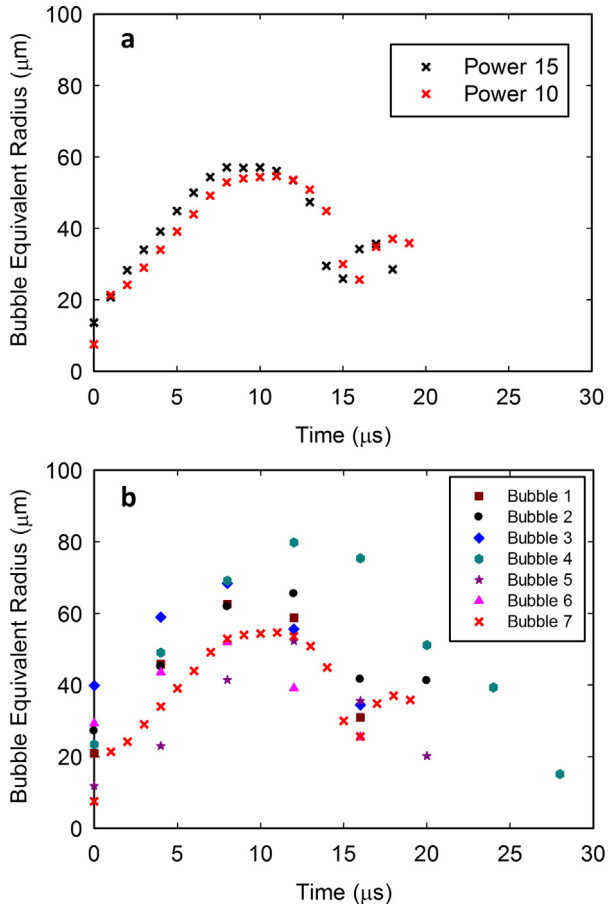

Fig. 7. (a) Bubble equivalent radius plotted over time for single bubbles around tip 10P at power 10 and power 15. Extracted from images taken at 1 million fps (b) Bubble equivalent radius over time for single bubbles around tip 10P at power 10. The cross symbol plot is the same at in (a) at 1 million fps, the others are from images sequences done at 250 kfps.

the original cropped bubble images. The corresponding original image sequence in Fig. 6(d) shows the individual bubble growing and collapsing near the end of tip 10P.

Out of the bubbles analysed, the maximum radius ranged from ~40 μm to ~80 μm (Fig. 7). It increased over time before reaching a peak and decreasing rapidly when the bubbles collapsed. The speed of bubbles remained constant for the first half of the growth cycle and then increased rapidly during the collapse phase, as expected. The maximum bubble speed observed was $27 \pm 7\ \mathrm{ms}^{-1}$.

4. Discussion

High speed imaging of ultrasonic scalers showed that whilst the majority of cavitation is in the form of clouds, individual microbubbles were also observed. Image analysis and manual tracking enabled bubble radius and speed to be calculated at various points in their life cycle.

The scaler tip was operated at 29 KHz giving an oscillation period of approximately 34 μs. The oscillation period of the single microbubbles ranged from 16 to 20 μs (Fig. 7). Therefore one acoustic cycle is equal to two deformation cycles of a bubble.

At power 5 bubbles appear at one point on the end of the scaler tip. They may have occurred at this point in particular because that is the location of the pressure antinode at that power setting.

Cavitation bubbles grow above the tip just as it reaches its maximum amplitude whilst moving upwards, and continue to grow larger as the tip moves downwards (Figs. 2 & 5). They then collapse when the tip reaches its maximum amplitude whilst moving downward or as soon as it starts to move upward. This shows that the rarefaction phase of low pressure happens on the side which the scaler is receding from. This was also observed for bubble clouds. Therefore bubbles collapse on one side of the scaler tip whilst others grow on the other side, and this reverses at the tip moves.

The bubble collapse happens much faster than the growth phase so the micro-jet cannot be visualised in this set of images taken at 250 kfps. In this case the closest boundary was the ultrasonic scaler tip itself so the bubble collapsed onto the tip.

All individual bubbles analysed in this study collapsed asymmetrically (Fig. 4). This suggests that they were influenced by proximity to the scaler tip or to other bubbles, since bubble collapse near a boundary is asymmetric [8]. This can also be seen in supplementary video S2 where the bubble moved upwards before it collapsed. This occurred because it was attracted to the bubble cloud above it which can be seen in Fig. 5. This in line with theoretical calculations which show that collapse propagates from the outer bubbles to the centre of a bubble cloud [34]. Video S2 shows a group of individual bubbles which was occasionally observed. This behaviour was not common but shows how individual bubbles behave in proximity to each other. Bubbles most commonly occurred as clouds, which have been investigated in our previous paper Vyas et al. [30].

The high ICC value shows good inter-operator reliability in manually tracking the bubble growth and collapse using the MTrackJ plugin, therefore this method is reproducible. The dot plot (Fig. 6b) further demonstrates good agreement between the different speeds measured by the different operators.

Two bubbles analysed at different power settings had similar radii (Fig. 7a) but larger bubbles can be seen at higher power settings in Fig. 3. Therefore although this work shows that increasing power causes an increase in the quantity of cavitation microbubbles, further research is needed to confirm how the power of the scaler affects their size. The maximum speed of the bubbles recorded was $27 \pm 7\ \mathrm{ms}^{-1}$ during the collapse phase. Collapse speeds were similar at the medium and high power settings.

This work can be improved and further developed in several ways. The radii produced by ultrasonic scaling and endodontic instruments have not previously been published therefore it is difficult to compare these results with previous studies. Future work can involve comparing experimental results to theoretical predictions. Most high speed imaging studies of cavitation microbubbles use laser generated bubbles whose sizes and locations can be precisely controlled. As we have imaged cavitation occurring around a clinical instrument, it is difficult to localise the bubble dynamics, making it challenging to image individual bubbles in the restricted field of view of the Photron camera. In addition many individual bubbles were obscured by the bubble clouds so their outline could not be extracted using the image analysis procedure used in the study. This meant that only a small number of cavitation bubbles could be analysed and therefore the samples may not be representative. Further work can be done using the methods established in this study to analyse bubble microjets and their effect on biofilm removal.

5. Conclusions

In conclusion, this study has highlighted the usefulness of image processing and high speed imaging in evaluating cavitation around ultrasonic scalers. Cavitation bubble dynamics around ultrasonic scalers have been visualised and analysed to show the average sizes of microbubbles and their size and speed during var-

ious phases of their life cycle. These insights could help to create instruments which produce optimal cavitation bubbles for biofilm removal.

Acknowledgements

NV gratefully acknowledges financial support from the EPSRC through a studentship from the PSIBS Doctoral Training Centre (EP/F50053X/1), and the loan of the Photron SA 1.1 and Shimadzu HPV 1 high speed cameras from the EPSRC Engineering Instrument Pool. The authors acknowledge helpful discussions with the late Professor J. R. Blake (University of Birmingham).

Appendix A. Supplementary material

Supplementary data associated with this article can be found, in the online version, at http://dx.doi.org/10.1016/j.ultras.2017.05.015.

References

[1] B. Verhaagen, D.F. Rivas, Measuring cavitation and its cleaning effect, Ultrason. Sonochem. 29 (2016) 619–628.
[2] A.D. Walmsley, et al., Identifying cavitation around dental ultrasonic instruments, in: 39th International Congress on Noise Control Engineering (2010), INTER-NOISE.
[3] A.D. Walmsley et al., Advances in power driven pocket/root instrumentation, J. Clin. Periodontol. 35 (s8) (2008) 22–28.
[4] G. Duhar, C. Colin, Dynamics of bubble growth and detachment in a viscous shear flow, Phys. Fluids (1994-present) 18 (7) (2006) 077101.
[5] R. Maurus, V. Ilchenko, T. Sattelmayer, Automated high-speed video analysis of the bubble dynamics in subcooled flow boiling, Int. J. Heat Fluid Flow 25 (2) (2004) 149–158.
[6] T.W. Asegehegn, M. Schreiber, H.J. Krautz, Investigation of bubble behavior in fluidized beds with and without immersed horizontal tubes using a digital image analysis technique, Powder Technol. 210 (3) (2011) 248–260.
[7] V. Garbin et al., Changes in microbubble dynamics near a boundary revealed by combined optical micromanipulation and high-speed imaging, Appl. Phys. Lett. 90 (11) (2007) 114103.
[8] C.E. Brennen, Cavitation and Bubble Dynamics, Cambridge University Press, 2013, p. 269.
[9] P. Tho, R. Manasseh, A. Ooi, Cavitation microstreaming patterns in single and multiple bubble systems, J. Fluid Mech. 576 (2007) 191–233.
[10] Y. Tomita et al., Growth and collapse of cavitation bubbles near a curved rigid boundary, J. Fluid Mech. 466 (2002) 259–283.
[11] D.F. Gaitan et al., Sonoluminescence and bubble dynamics for a single, stable, cavitation bubble, J. Acoust. Soc. Am. 91 (6) (1992) 3166–3183.
[12] W. Lauterborn et al., Acoustic cavitation, bubble dynamics and sonoluminescence, Ultrason. Sonochem. 14 (2007) 484–491.
[13] J.R. Blake, D.C. Gibson, Cavitation bubbles near boundaries, Annu. Rev. Fluid Mech. 19 (1) (1987) 99–123.
[14] Y. Matsumoto, S. Yoshizawa, Behaviour of a bubble cluster in an ultrasound field, Int. J. Numer. Meth. Fluids 47 (6–7) (2005) 591–601.
[15] A.A. Doinikov, Bjerknes forces and translational bubble dynamics. Bubble and Particle Dynamics in Acoustic Fields: Modern Trends and Applications (2005), 95-143.
[16] M.S. Plesset, A. Prosperetti, Bubble dynamics and cavitation, Annu. Rev. Fluid Mech. 9 (1) (1977) 145–185.
[17] G.L. Chahine et al., Modeling of surface cleaning by cavitation bubble dynamics and collapse, Ultrason. Sonochem. 29 (2016) 528–549.
[18] O. Shpak et al., The role of gas in ultrasonically driven vapor bubble growth, Phys. Med. Biol. 58 (8) (2013) 2523.
[19] A. Philipp, W. Lauterborn, Cavitation erosion by single laser-produced bubbles, J. Fluid Mech. 361 (1998) 75–116.
[20] M. Erriu et al., Microbial biofilm modulation by ultrasound: current concepts and controversies, Ultrason. Sonochem. 21 (2014) 15–22.
[21] M. Versluis, High-speed imaging in fluids, Exp. Fluids 54 (2) (2013) 1458.
[22] B. Verhaagen et al., Acoustic streaming induced by an ultrasonically oscillating endodontic file, J. Acoust. Soc. Am. 135 (4) (2014) 1717–1730.
[23] H.H. Peeters et al., Visualization of removal of trapped air from the apical region of the straight root canal models generating 2-phase intermittent counter flow during ultrasonically activated irrigation, J. Endodont. 40 (6) (2014) 857–861.
[24] J. Blanken et al., Laser induced explosive vapor and cavitation resulting in effective irrigation of the root canal. Part 1: a visualization study, Lasers Surg. Med. 41 (7) (2009) 514–519.
[25] L.-M. Jiang et al., Evaluation of a sonic device designed to activate irrigant in the root canal, J. Endodont. 36 (1) (2010) 143–146.
[26] H. Matsumoto, Y. Yoshimine, A. Akamine, Visualization of irrigant flow and cavitation induced by Er: YAG laser within a root canal model, J. Endodont. 37 (6) (2011) 839–843.
[27] R.G. Macedo et al., Sonochemical and high-speed optical characterization of cavitation generated by an ultrasonically oscillating dental file in root canal models, Ultrason. Sonochem. 21 (2014) 324–335.
[28] A.D. Walmsley, W.R.E. Laird, A.R. Williams, Displacement amplitude as a measure of the acoustic output of ultrasonic scalers, Dent. Mater. 2 (1986) 97–100.
[29] A.R. Williams, A. Walmsley, Exposimetry of low-frequency ultrasonic dental devices, IEEE Trans. Ultrason. Ferroelectr. Freq. Control 35 (2) (1988) 264–269.
[30] N. Vyas et al., High speed imaging of cavitation around dental ultrasonic scaler tips, PLoS One 11 (3) (2016) e0149804.
[31] J. Schindelin et al., Fiji: an open-source platform for biological-image analysis, Nat. Methods 9 (7) (2012) 676–682.
[32] I. Arganda-Carreras, et al., Trainable weka segmentation, http://fiji.sc/Trainable_Weka_Segmentation, 2013, Accessed 07.09.2016.
[33] E. Meijering, O. Dzyubachyk, I. Smal, Methods for cell and particle tracking, Methods Enzymol. 504 (9) (2012) 183–200.
[34] J.R. Blake et al., Acoustic cavitation: the fluid dynamics of non–spherical bubbles, Philos. Trans. R. Soc. London, A: Math., Phys. Eng. Sci. 357 (1751) (1999) 251–267.